Chemical Bath Deposition of α-GaOOH with Tunable Morphology on Silicon Using the pH Adjustment

Guislain Hector, Estelle Appert, Herve Roussel, Isabelle Gélard, Vincent Consonni

Chemical Bath Deposition of α-GaOOH with Tunable Morphology on Silicon Using the pH Adjustment

Guislain Hector,[1] Estelle Appert,[1] Hervé Roussel,[1] Isabelle Gélard,[1] and Vincent Consonni[1*]

[1] Université Grenoble Alpes, CNRS, Grenoble INP, LMGP, F-38000 Grenoble, France

CORRESPONDING AUTHOR FOOTNOTE:

*E-mail: vincent.consonni@grenoble-inp.fr

ABSTRACT

The growth of GaOOH by chemical bath deposition has received a great attention over the past years as a first step to form Ga_2O_3 with the α- or β-phases by combining a wet chemical route with a thermal annealing in air. By using gallium nitrate and sodium hydroxide in aqueous solution, we show that the structural morphology of GaOOH deposits is thoroughly tunable both in terms of dimensions, density and nature by varying the initial pH value from acidic to basic conditions. In the low-pH region associated with a low supersaturation level and where Ga^{3+} ions represent the dominant Ga(III) species, GaOOH microrods with a low aspect ratio and low density prevail. In the intermediate-pH region associated with a high supersaturation level and where $GaOH^{2+}$ ions represent the dominant Ga(III) species, GaOOH prismatic nanorods with a high aspect ratio and high density are preferentially formed. In the high-pH region where $Ga(OH)_4^-$ complexes are predominantly formed, the growth of partially crystallized GaOOH thin films with a typical thickness of about 1 μm proceeds. These findings show the correlation between the characteristics of the chemical bath and the resulting structural morphology of GaOOH deposits. They further open great perspectives to grow GaOOH and hence Ga_2O_3-based materials on silicon with a dedicated structural morphology using chemical bath deposition for

engineering devices in the fields of gas sensing, solar-blind UV-C photo-detection, and power electronics.

1. INTRODUCTION

Gallium oxide (Ga_2O_3) crystallizing into the β-phase has emerged as a promising ultra-wide band gap semiconductor for gas sensing, solar blind UV-C photo-detection, and power electronics owing to its long-term stability, its high melting point, its high breakdown electric field, and its relatively high electron mobility.[1-4] The growth of β-Ga_2O_3 thin films and nanostructures has been achieved by a wide variety of physical and chemical vapor deposition techniques, such as molecular beam epitaxy,[5] pulsed laser deposition,[6] chemical vapor deposition,[7] metal-organic chemical vapor deposition,[8] and atomic layer deposition.[9] Alternatively, several chemical deposition techniques in solution have been developed to grow β-Ga_2O_3 thin films and nanostructures, including sol-gel process, hydrothermal synthesis, and chemical bath deposition (CBD).[10-15]

The CBD process using gallium nitrate ($Ga(NO_3)_3$) in an aqueous solution and working at low temperature (< 100 °C) and at atmospheric pressure is considered as a low-cost, surface scalable, and easily implemented process,[16] which is in line with the development of green chemistry.[17] The growth of β-Ga_2O_3 thin films and nanostructures relies on a double-step process, consisting in initially forming Ga(III) oxide-hydroxide (GaOOH) thin films and nanostructures using CBD and subsequently converting them into β-Ga_2O_3 thin films and nanostructures using thermal annealing at high temperature in air.[16] The first step using CBD basically governs the shape and size of the resulting nanostructures, while the second step using thermal annealing controls their crystalline phase. By using that double step-process, a large number of nanostructures with different shapes and sizes has been formed using the homogeneous growth in bulk solution. Recently, significant efforts have been devoted to optimizing the heterogeneous growth on dedicated substrates to facilitate the integration of β-Ga_2O_3 thin films and nanostructures into engineering devices. Fujihara *et al.* reported the heterogeneous growth of GaOOH particles on different oxide and fluoride substrates using $Ga(NO_3)_3$ as the chemical precursor, showing that their formation is promoted on TiO_2, MgO, and SnO_2/SnO_2:F substrates.[18] Liang *et al.* reported the heterogeneous growth of GaOOH nanorods on SnO_2:F substrates using $Ga(NO_3)_3$ and urea as the chemical precursors under static and dynamic conditions, revealing that their formation may be driven by screw dislocations.[19] Alternatively, Hector *et al.* investigated the heterogeneous growth of GaOOH microrods on silicon and showed the effects of the $Ga(NO_3)_3$ concentration on their shape and

dimensions.[20] The formation of GaOOH plate-layered rods, round-plate rods, and round-rods was shown by increasing the $Ga(NO_3)_3$ concentration and their properties were correlated with the supersaturation level in the chemical bath as deduced from thermodynamic computations. Although these GaOOH microrods converted into β-Ga_2O_3 microrods are of interest, it is highly desirable to further optimize their shape and dimensions on silicon during the CBD process. In that respect, the effects of the pH in the chemical bath has never been explored despite its primary importance when using the CBD process in aqueous solution.

In this work, we investigate the effect of the initial pH (pH_0) value varying from acidic to basic conditions on the growth of GaOOH by CBD on silicon using $Ga(NO_3)_3$ and sodium hydroxide (NaOH) as chemical precursors in aqueous solution. The dimensions, density, and nature of GaOOH deposits are found to strongly depend on the pH_0 value and to be correlated with the nature of the dominant Ga(III) species in aqueous solution and the supersaturation level as determined from thermodynamic computations.

2. EXPERIMENTAL DETAILS

2.1. Deposition Techniques. GaOOH deposits were grown on silicon by CBD using a pH_0 fixed method. Prior to the process, the Si(001) substrates were cleaned with acetone (acetone ≥ 99.8%, VWR, CAS: 67-64-1) and isopropyl alcohol (isopropanol ACS reagent ≥ 99.8%, Sigma-Aldrich, CAS: 67-63-0) in a sonication bath to remove organic pollutants. The deposits were grown by CBD using an aqueous solution containing gallium nitrate hydrate ($Ga(NO_3)_3 \cdot x H_2O$, 99.9%, Sigma-Aldrich, CAS: 69365-72-6) with x considered as 8,[21] and using the addition of sodium hydroxide (NaOH, Sigma-Aldrich, CAS: 1310-73-2) to vary the pH_0 value in the range of 2.26-10.92. All chemical precursor solutions were prepared by dissolving 16 mM of $Ga(NO_3)_3$ in ultrapure water. To ensure the complete dissolution of $Ga(NO_3)_3$, the solutions were placed on a hot plate and magnetically stirred at 70 °C for 12 h. The Si(001) substrates were then placed face down in a sealed reactor containing the $Ga(NO_3)_3$ solution and the proper amount of NaOH to fix the pH_0 value. The NaOH concentration was set to 0, 20.6, 33.8, 38.5, 41.2, 42.1, 44.0, 46.7, 52.1 and 60.2 mM for a pH_0 value of 2.26, 2.72, 3.00, 3.35, 3.79, 4.16, 6.29, 7.46, 9.15 and 10.92, respectively. The reactor was placed in a regular oven kept at 70 °C for 24 h. At the end

of the CBD process, the Si(001) substrates were washed with distilled water and dried under a flow of nitrogen.

Characterization Techniques. The morphological properties of deposits were investigated using a ZEISS Gemini 300 field-emission scanning electron microscopy (FESEM) instrument (Carl Zeiss, Oberkochen, Germany). The dimensions of microrods and prismatic nanorods were measured on the FESEM images by using ImageJ software, where their diameter and length were determined over a population of at least 50 objects. XRD patterns were collected with a BRUKER D8 Advance diffractometer using Cu $K\alpha_1$ radiation according to the Bragg−Brentano configuration. Raman spectra were acquired with a HORIBA/JOBIN YVON Labram spectrometer equipped with a liquid-nitrogen-cooled CCD detector. A 488 nm Ar^+ laser line with a power on the surface of the sample around 1 mW was used to collect the Raman spectra over the range of 2750–3500 cm^{-1}. The laser was focused with a 100 × objective to obtain a spot size of about 1 μm^2. All the Raman spectra were calibrated with a silicon reference sample considering the theoretical Raman line set to 520.7 cm^{-1}. EDS spectra were recorded with a BRUKER X-ray detector incorporated in the ZEISS Gemini 300 FESEM instrument operating at 5 and 15 kV.

Thermodynamic Computations. Thermodynamic calculations were performed with Visual MINTEQ software for the determination of the speciation diagrams of Ga(III) species as well as the theoretical solubility plots of GaOOH at 70 °C for each growth condition (*i.e.*, with varying pH_0 value obtained by adding NaOH). The formation of hydroxide complexes between the single metallic cations in aqueous solution (Ga^{3+} ions), denoted as $M^{x+,}$ and the single possible ligands (HO^- ions), denoted as L, occurs according to the general reactions: $nM^{x+} + iL \leftrightarrow M_nLi^{nx+}$,where M_nLi^{nx+} is the complex considered, i is the coordination number, and x is the cation charge. The related stability constants β_i^L associated with each reaction are given by $\beta_i^L = \frac{[M_n L_i^{nx+}]}{[M^{x+}]^n [L]^i}$. These constants were taken at 25 °C from NIST for Ga(III) species, as recapitulated in Ref. 20 . The constants at 70°C were deduced from the Van't Hoff relation. The calculation of the theoretical solubility plots for each growth condition was achieved by taking into account the GaOOH(s) and $Ga(OH)_3$ (am) solid phases using the solubility constants presented in Ref. 20.

3. RESULTS AND DISCUSSION

3.1. Effects of the pH_0 on the Morphological and Structural Properties of Deposits. The morphological properties of deposits grown by CBD with a pH_0 value ranging from 2.26 to 10.92 are presented in **Figure 1** using FESEM imaging**.**

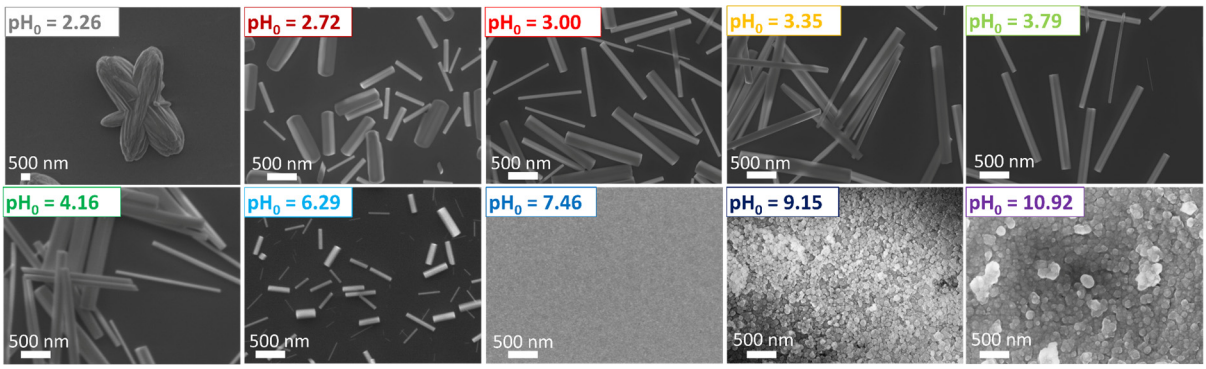

Figure 1. Top-view FESEM images of deposits grown by CBD with a pH_0 value of 2.26, 2.72, 3.00, 3.35, 3.79, 4.16, 6.29, 7.46, 9.15, and 10.92.

Depending on the pH_0 value, the structural morphology of deposits changes from microrods through prismatic nanorods to thin films. When no NaOH is added to the chemical bath, a pH_0 value of 2.26 was measured and microrods as plate-layered rods are formed, as reported in Ref. 20. These microrods are composed of the stack of thin, round plates with the possible occurrence of few secondary nucleation places at their base and are inclined according to a random tilt angle, as shown in **Figure 2a,b**. The formation of prismatic nanorods lying horizontally on the surface occurs as the pH_0 value is increased to 2.72, as presented in **Figure 2c,d**. Here, two populations of objects are detected, typically microrods and prismatic nanorods. In the pH_0 value range of 3.00–6.29, the formation of prismatic nanorods prevails over the formation of microrods. This type of prismatic nanorods has also been reported during the homogeneous growth of GaOOH by CBD.[11] In contrast, the formation of continuous thin films composed of coalesced spherical nanoparticles is revealed as the pH_0 value is further increased to 7.46, 9.15, and 10.92. In summary, the acidic domain of pH_0 leads to the formation of microrods and prismatic nanorods, while the basic domain of pH_0 results in the formation of coalesced spherical nanoparticle thin films.

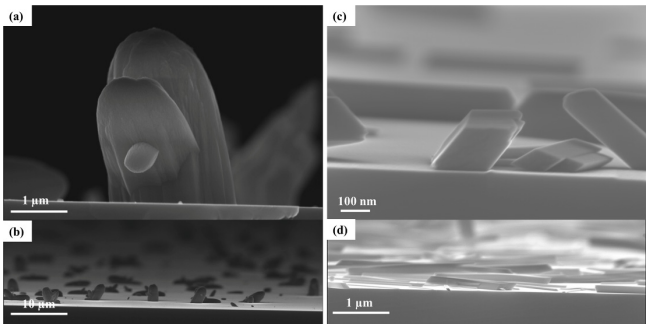

Figure 2. Cross-sectional view FESEM images of (a,b) microrods, and (c,d) prismatic nanorods grown by CBD. (a,c) and (b,d) correspond to high and low magnification images, respectively.

The mean length, mean diameter, aspect ratio, and apparent density of microrods and prismatic nanorods are presented in **Figure 3a-d** and strongly depend on the pH_0 value**.** When no NaOH is added to the chemical bath, the microrods exhibit a mean length of about 5.40 µm and a mean diameter of about 1.70 µm, leading to an aspect ratio of around 3.25. The apparent density of microrods is very low, on average less than one object per 100 μm^2. In contrast, when NaOH is added to the chemical bath to adjust the pH_0 value, the prismatic nanorods starts to form and the resulting mean dimensions are much smaller, while the density of objects is much higher. For a pH_0 value of 2.72, the microrods have a decreased mean length of about 856 nm and a decreased mean diameter of about 285 nm, resulting in an aspect ratio of around 3.07. The prismatic nanorods exhibit a mean length of about 556 nm and a mean diameter of about 92 nm, leading to a higher aspect ratio of about 6.35. The density of mirorods and prismatic nanorods jumps to a value of around 100 objects per 100 μm^2. As the pH_0 value is increased to 4.16, the mean length of prismatic nanorods significantly increases to reach the value of about 2.18 µm. In contrast, the mean diameter of prismatic nanorods only increases slightly to reach the value of about 196 nm. The increase in the mean length is thus more pronounced than the increase in the mean diameter, such that the aspect ratio initially increases strongly to the value of 13.0 at the pH_0 value of 3.00 and then saturates to the present value. However, for a pH_0 value of 6.29, the mean length and mean diameter of prismatic nanorods significantly decrease and reach the values of 390 nm and 99 nm, respectively, resulting in a decrease in the aspect ratio to around 5.57. Eventually, the apparent density of prismatic nanorods follows a particular evolution. It first increases strongly to the value of 255 objects per 100 μm^2 as the pH_0 value reaches 3.00, and second decreases drastically to the value of

45 objects per 100 µm^2 as the pH_0 value reaches 3.79. Finally, it drastically increases to a mean value of 366 objects per 100 µm² as the pH_0 value reaches 6.29.

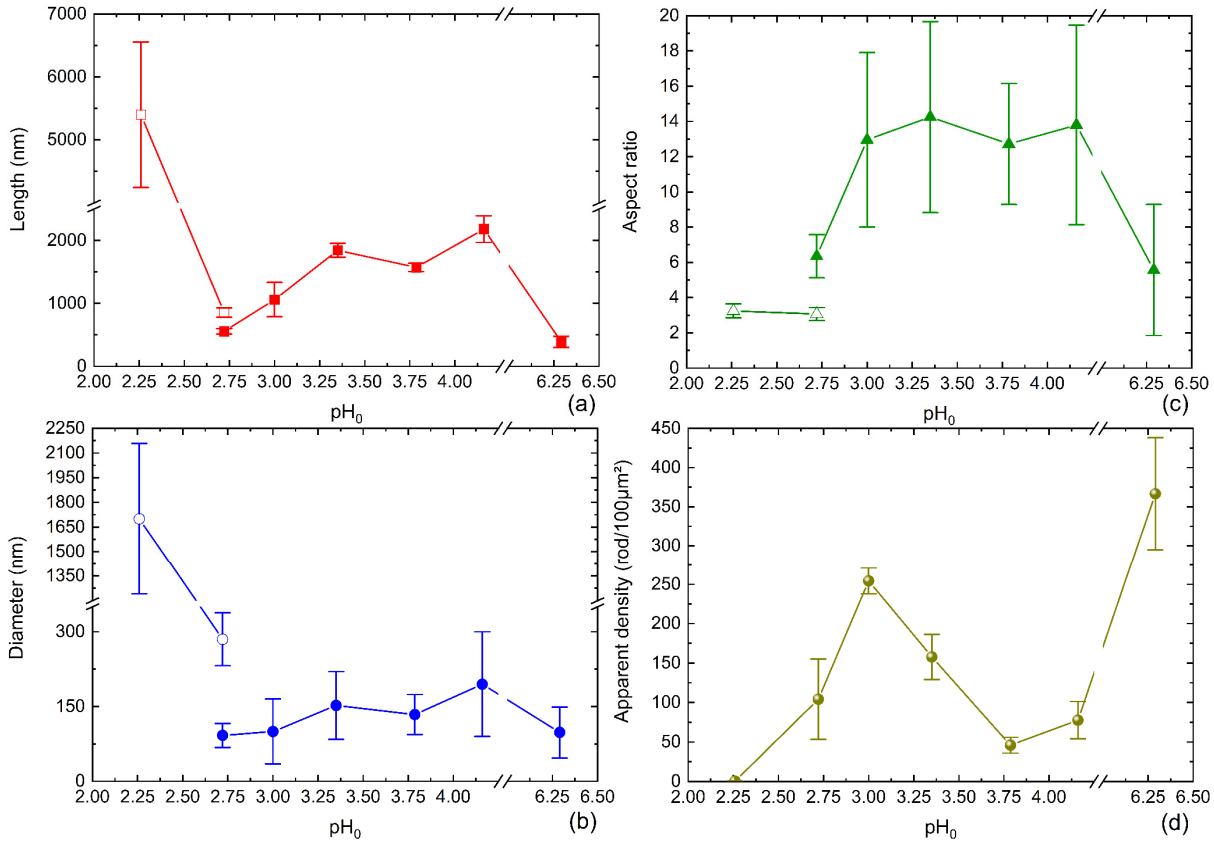

Figure 3. Evolutions of the (a) mean length, (b) mean diameter, (c) aspect ratio and (d) apparent density of microrods and prismatic nanorods grown by CBD as a function of the pH_0 value. The first population (open symbols) corresponds to microrods, while the second population (full symbols) corresponds to prismatic nanorods.

For a pH_0 value of 7.46, the film thickness is close to 400 nm and the nanoparticle size is estimated below 10 nm. The film becomes micrometer-thick with the increase of the concentration of NaOH. The film thickness at the pH_0 values of 9.15 and 10.92 was measured between 1 and 1.5 µm, while the nanoparticle size lies in the ranges of 20–35 and 30–120 nm, respectively. The crystallographic structure of deposits grown by CBD with a pH_0 value ranging from 2.26 to 10.92 was analyzed by XRD measurements, as presented in **Figure 4a**. On the one hand, the XRD patterns show that both microrods and prismatic nanorods crystallize into the α-GaOOH orthorhombic phase belonging to the *Pnma* space group and corresponding to the calculated ICDD 04-010-9861 file. The XRD patterns of microrods are marked by the presence of (200), (101), (201), (301), (210), (400), (111), (211), (401), (202), (311),

(501), (112), (212), (402), (600), (312), (511), and (020) diffraction peaks pointing at 18.11, 21.65, 26.83, 33.86, 35.29, 36.69, 37.32, 40.70, 41.95, 44.12, 45.88, 50.78, 51.63, 54.29, 55.30, 56.33, 58.55, 60.12, and 62.42°. In order to assess the growth texture of microrods, the texture coefficients for each plane (C_{hkl}) and the degree of preferred orientation (σ) were estimated from the XRD patterns using the Harris method[20] and are recapitulated in **Table S1** of Supporting Information. The intensity of each diffraction peak was determined after subtracting the background. The preferential growth directions of microrods correspond to the directions normal to the (200) and (101) planes with related texture coefficients of around 2.19 and 6.98, respectively ($C_{hkl\max}$ = 15). A proportion of about 15 and 47% of microrods is thus grown with the directions normal to the (200) and (101) planes, respectively. The degree of preferred orientation of microrods is medium with a value of about 1.68 ($\sigma_{\max}$ = 3.74). This indicates that the microrods have an intermediate growth texture, which is in agreement with the structural morphology as presented in **Figure 1**. In contrast, the XRD patterns of prismatic nanorods are exclusively dominated by the (101) and (202) diffraction peaks pointing at 21.65 and 44.12 °. This shows that prismatic nanorods grow with the (101) plane parallel to the surface, likely according to the growth axis aligned along the *b*-axis in the plane. The α-GaOOH orthorhombic phase of microrods and prismatic nanorods is further supported in **Figure 4b** through the related Raman spectra, revealing the occurrence of several lines pointed at 2848, 2890, 2922, and 2957 cm^{-1} and assigned to the corresponding OH stretching vibrations.[22] On the other hand, the XRD signal is much weaker, when the deposits form coalesced spherical nanoparticle thin films. The occurrence of the broad band at around 22.5° in the deposit grown with a pH_0 value of 9.15 indicates the formation of a partially crystallized thin film. The chemical composition of the partially crystallized thin films reveals the presence of Ga through the detection of the Ga L_α and K_α lines at 1.1 and 9.25 keV, respectively, as presented in **Figure S1** of Supporting Information. Interestingly, the occurrence of several Raman lines pointed at 2848, 2890, 2922, and 2957 cm^{-1} and assigned to the corresponding OH stretching vibrations again supports that the thin films are partially crystallized into the α-GaOOH orthorhombic phase.[22] It is worth noticing here that no Raman lines corresponding to the $Ga(OH)_3$ phase in microrods, prismatic nanorods, and partially crystallized thin films are detected.[23] This shows that the α-GaOOH orthorhombic phase is preferentially formed in the present CBD conditions and is relatively pure with no trace of the crystalline

$Ga(OH)_3$ phase. Nevertheless, the presence of the amorphous $Ga(OH)_3$ phase as residues cannot be excluded, specifically when the partially crystallized α-GaOOH thin films are deposited.

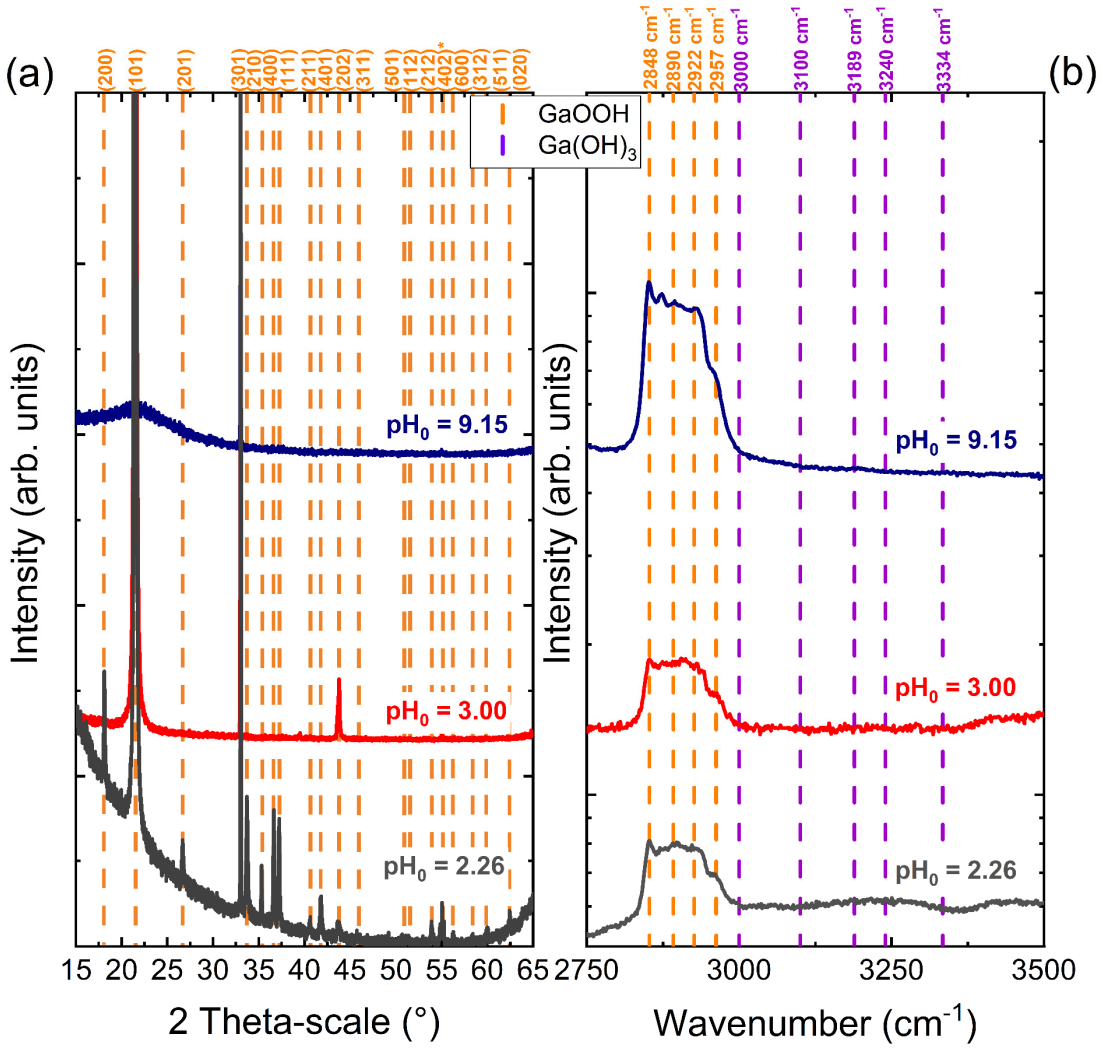

Figure 4. (a) XRD patterns of deposits grown by CBD with a pH_0 value of 2.26, 3.00, and 9.15, corresponding to microrods, prismatic nanorods, and thin films, respectively. The orange dashed lines correspond to the diffraction peaks of the α-GaOOH phase according to the ICDD 04-010-9861 file. The star symbol denotes for an artifact coming from the holder and superimposing to the diffraction peak. (b) Raman spectra of deposits grown by CBD with a pH_0 value of 2.26, 3.00, and 9.15, corresponding to microrods, prismatic nanorods, and thin films, respectively. The orange and purple dashed lines correspond to the phonon modes of the α-GaOOH and $Ga(OH)_3$ phases according to Ref. 22 and 23, respectively.

3.2. Effects of the pH_0 on the Nature of Ga(III) Species and Supersaturation. In order to show the physicochemical processes in the chemical bath driving the formation of α-GaOOH microrods, α-GaOOH prismatic nanorods and partially crystallized α-GaOOH thin films during the CBD process,

the speciation diagram of Ga(III) species along with the theoretical solubility plot are presented in **Figure 5a,b**. The curves were deduced from the equilibrium calculation for each pH value at 70 °C ranging from 1 to 12 with a 0.001 incremental step and by considering the following Ga(III) species and solid phases: Ga^{3+}, $GaOH^{2+}$, $Ga(OH)_2^+$, $Ga(OH)_4^-$, $Ga(OH)_{3(am)}$, and $GaOOH_{(s)}$.[24]

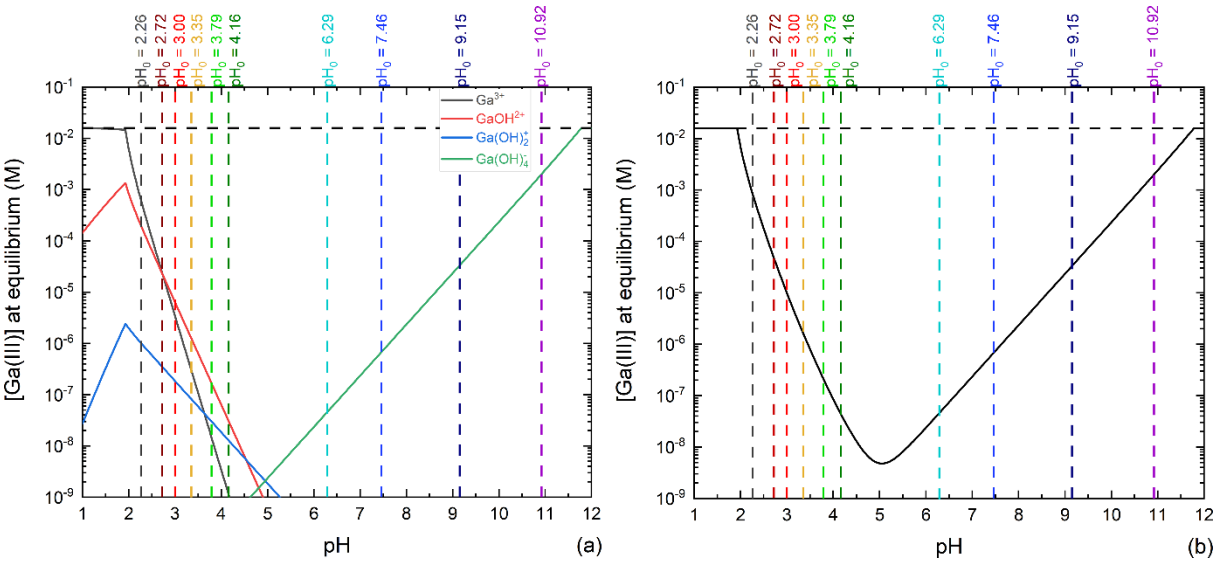

Figure 5. (a) Speciation diagram of Ga(III) species and (b) theoretical solubility plot of Ga(III) species at 70 °C as a function of pH, as computed by Visual MINTEQ software. The initial concentration of $Ga(NO_3)_3$ was set to 16 mM and is represented with the horizontal black dashed line.

The predominant Ga(III) species in the chemical bath are found to strongly depend on the pH as seen in **Figure 5a** and to affect the structural morphology of deposits. In the acidic domain of pH ranging from 1 to 2.75, Ga^{3+} ions are largely prevalent. However, in the acidic domain of pH ranging from 2.75 to 4.55, $GaOH^{2+}$ complexes get predominant. As the pH is further increased from 4.55 to 4.95, $Ga(OH)_2^+$ complexes are preferentially formed. Eventually, $Ga(OH)_4^-$ complexes are largely prevalent in the neutral and basic domains of pH ranging from 4.95 to 12. Very interestingly, each deposit with a different structural morphology thus proceeds in a pH value range where the predominant Ga(III) species differ. A schematic diagram recapitulating the structural morphology and dimensions of deposits as a function of the pH_0 value is presented in **Figure 6**.

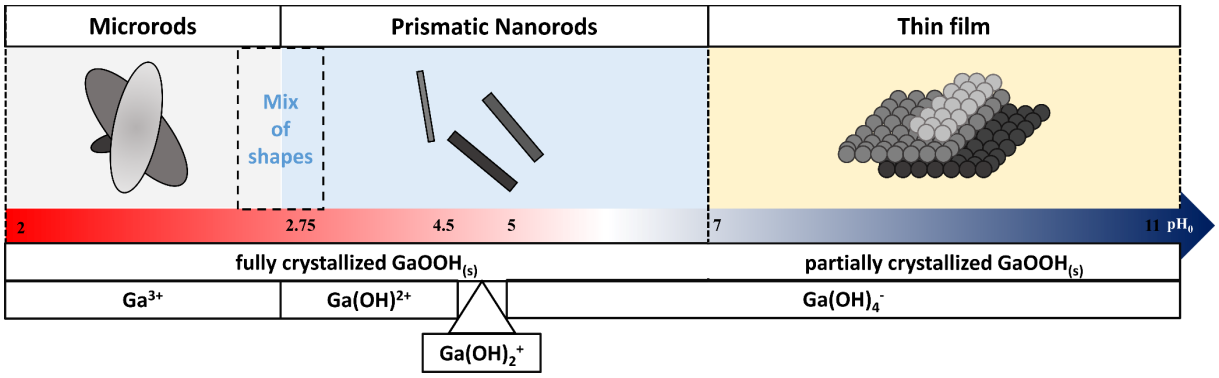

Figure 6. Schematic diagram showing the structural morphology and dimensions of deposits as a function of the pH_0 value and their relationship with the predominant Ga(III) species in the chemical bath.

The α-GaOOH microrods and α-GaOOH prismatic nanorods are preferentially formed when Ga^{3+} ions and $GaOH^{2+}$ complexes predominate in the chemical bath, respectively. The precipitation mechanism of GaOOH in aqueous solution in the acidic domain of pH below a pH_0 value of 4.55 may be driven by the forced hydrolysis of Ga^{3+} ions as proposed by Tas *et al.*[11] and of $GaOH^{2+}$ complexes as follows:[24]

$$Ga^{3+} + 2H_2O \rightarrow GaOOH_{(s)} + 3H^+ \quad (1)$$

$$GaOH^{2+} + H_2O \rightarrow GaOOH_{(s)} + 2H^+ \quad (2)$$

The Gibbs free energy of reaction at 25°C and 1 atm was estimated to ΔrG = -789.57 kcal.mol^{-1} and ΔrG = -529.57 kcal.mol^{-1} for **Eq. 1** and **Eq. 2**, respectively.[24] In that sense, the physicochemical process of forced hydrolysis in the chemical bath is favorable for the formation of α-GaOOH microrods and prismatic nanorods on silicon. The two different shapes obtained when using Ga^{3+} ions and $GaOH^{2+}$ complexes as the predominant Ga(III) species may come from the distinct chemical and electrostatic interactions occurring with the different growing planes. This type of physicochemical processes has largely been documented in the case of ZnO nanostructures,[25] where their shape and aspect ratio can finely be tuned depending on the additives and their concentration in the chemical bath.[26-29] It should be noted here that the transition from microrods to prismatic nanorods is not abrupt because both Ga^{3+} ions and $GaOH^{2+}$ complexes coexist in the chemical bath for a pH_0 value of around 2.72. Moreover, the α-GaOOH prismatic nanorods also form when $Ga(OH)_2^+$ and $Ga(OH)_4^-$ complexes predominate in the chemical bath. The precipitation mechanism of GaOOH in aqueous solution in the acidic and neutral

domains of pH for a pH_0 value ranging from 4.55 to about 7 may proceed through additional dehydroxylation and dehydration processes. In contrast, the partially crystallized α-GaOOH thin films are preferentially formed in the basic domain of pH for a pH_0 value ranging from about 7 to 10.92, where $Ga(OH)_4^-$ complexes exclusively predominate in the chemical bath. The partially crystallized thin films are expected to form following a double step process, consisting in preferentially growing i) amorphous $Ga(OH)_3$ in a first step through a dehydroxylation process (**Eq. 3**), and ii) GaOOH in a second step through a dehydration process (**Eq. 4**):[24, 30-31]

$$Ga(OH)_4^- \rightarrow Ga(OH)_{3\ (am)} + HO^- \quad (3)$$

$$Ga(OH)_{3\ (am)} \rightarrow GaOOH_{(s)} + H_2O \quad (4)$$

It is worth noticing that the CBD conditions in terms of temperature, pH and time are liable to promote the formation of either the $Ga(OH)_3$ or GaOOH phases, or both of them.[31] In the present conditions using a relatively high temperature of 70 °C, a relatively high pH_0 value above 7, and a long time of 24 h, only the α-GaOOH phase is partially crystallized to form coalesced spherical nanoparticle thin films.

The use of classical nucleation and growth theory[32] to account for the dimensions and density of GaOOH microrods and prismatic nanorods and their evolution as a function of the pH_0 value requires the determination of a certain number of thermodynamic quantities. As discussed in Ref. 20, the dimensions (*i.e.*, diameter and length) of GaOOH microrods and prismatic nanorods are dependent upon the crystal growth rate G, which is directly related to the absolute supersaturation (S_A) as follows:[32]

$$G(S_A) = k_g S_A^g \quad (5)$$

where k_g and g are kinetic parameters such that $g = 1$ and k_g follows an Arrhenius law for a stoichiometric solution and a high supersaturation ratio (S_R) value. In contrast, the density of GaOOH microrods and prismatic nanorods depends on the heterogeneous nucleation rate (J_{HEN}), which is also directly related to S_R as follows:[32]

$$J_{HEN}(S_R) = A S_R e^{\frac{-B}{\ln^2(S_R)}} \quad (6)$$

where A is a kinetic parameter and B is a dimensionless thermodynamic parameter. J_{HEN} thus varies very strongly with S_R. For example, in the case of oxide precipitation in aqueous solution, a value of $S_R = 10$

typically leads to the formation of one nucleus per cm^3 in 10^{70} seconds, while a value of S_R = 100 typically leads to the formation of 10^5 nuclei per cm^3 in one second.[32] The values of the concentration of Ga(III) species at equilibrium (C^*), S_A, and S_R for pH_0 values ranging from 2.26 to 6.29 were estimated from **Figure 5b** and are reported in **Table 1**.

Table 1. Concentration of Ga(III) species at equilibrium C^*, S_A, and S_R for pH_0 values ranging from 2.26 to 4.16.

pH_0	C^* (mM)	S_A (mM)	S_R
2.26	$8.50 \cdot 10^{-1}$	15.150	18.82
2.72	$4.76 \cdot 10^{-2}$	15.952	336.4
3.00	$9.95 \cdot 10^{-3}$	15.990	1608
3.35	$1.65 \cdot 10^{-3}$	15.998	9712
3.79	$2.11 \cdot 10^{-4}$	16.000	75938
4.16	$4.45 \cdot 10^{-5}$	16.000	359829
6.29	$4.60 \cdot 10^{-5}$	16.000	347716

The concentration of Ga(III) species at equilibrium is low in the range of pH_0 values investigated and falls from $8.50 \cdot 10^{-1}$ to $4.45 \cdot 10^{-5}$ mM as the pH_0 value is increased from 2.26 to 4.16. As a result, S_A approaches the value of the initial concentration of $Ga(NO_3)_3$ of 16 mM and slightly increases from 15.150 to 16.000 mM. Correlatively following **Eq. 5**, the mean diameter and length of GaOOH prismatic nanorods as presented in **Figure 3a,b** continuously increase from 92 to 196 nm and from 556 nm to 2.18 µm, respectively. In contrast, S_R drastically increases from 18.82 to nearly 360000 as the pH_0 value is increased from 2.26 to 4.16. Correlatively following **Eq. 6**, the density of GaOOH microrods and prismatic nanorods as presented in **Figure 3d** jumps from an extremely low value of 0.5 objects per 100 μm^2 to 255 objects per 100 μm^2 as the pH_0 value is increased from 2.26 to 3.00. Nevertheless, the density of GaOOH prismatic nanorods decreases for pH_0 values greater than 3.00 owing to the competition between the heterogeneous nucleation and homogeneous nucleation processes in aqueous solution. When the value of S_R is very high, the homogeneous nucleation rate J_{HON} approaches J_{HEN} such that $J_{HON} \approx J_{HEN}$. In that case, the nucleation process takes place in the whole volume of the solution in a quasi-equivalent manner. The volume around the substrate being much lower than the volume of the reactor, for an equivalent nucleation rate, the number of nuclei formed is therefore lower. Consequently, the

density of GaOOH prismatic nanorods observed on the substrate following the heterogeneous nucleation process is lower. This phenomenon has commonly been observed during the heterogeneous nucleation process of other oxides including ZnO nanostructures.[33] From the experimental point of view, the first decrease in the density of GaOOH prismatic nanorods occurs when the value of $S_R \approx 10^4$ and the further decrease proceeds when the value of $S_R \approx 7.5 \cdot 10^4$. Importantly, the purely thermodynamic considerations cannot account for the mean diameter, mean length, and apparent density of GaOOH prismatic nanorods grown for a pH_0 value of 6.29, which is close to the transition towards the formation of partially crystallized GaOOH thin films. Kinetic considerations along with the change of the predominant Ga(III) species inducing a differential reactivity originating from distinct chemical and electrostatic interactions may also affect the nucleation and growth of GaOOH prismatic nanorods. For instance, the high density of GaOOH prismatic nanorods correlated with their low mean diameter and length indicate that the elongation process is limited by the diffusive transport of chemical reactants.[34] The present findings reveal that controlling the characteristics of the chemical bath in terms of the nature of the dominant Ga(III) species and of the supersaturation level is a powerful tool to tune the structural morphology of GaOOH deposits on silicon from microrods through prismatic nanorods to partially crystallized thin films. The control of the morphology of GaOOH deposits is of particular interest, since their structural conversion into β-Ga_2O_3 deposits readily operates at high temperature.[20] This opens great perspectives for the further integration of GaOOH and hence Ga_2O_3-based materials into engineering devices in the fields of gas sensing, solar-blind UV-C photo-detection, and power electronics.

4. CONCLUSIONS

In summary, we have developed the growth of GaOOH deposits by CBD on silicon using $Ga(NO_3)_3$ and NaOH as chemical precursors in aqueous solution and specifically investigated the effect of the pH_0 value varying from acidic to basic conditions. In the low-pH region where the supersaturation level is low and Ga^{3+} ions constitute the dominant Ga(III) species, α-GaOOH microrods with the orthorhombic phase exhibiting a low aspect ratio and low density are preferentially formed. In the intermediate-pH region where the supersaturation level is high and $GaOH^{2+}$ complexes constitute the dominant Ga(III) species, α-GaOOH prismatic nanorods with the orthorhombic phase and exhibiting a high aspect ratio and high density prevail. These α-GaOOH prismatic nanorods develop with the (101) plane parallel to

the surface according to the growth axis aligned along the *b*-axis in the plane. The formation of both GaOOH microrods and prismatic nanorods is expected to proceed through a forced hydrolysis process of Ga^{3+} ions and $GaOH^{2+}$ complexes. In the high-pH region where $Ga(OH)_4^-$ complexes constitute the dominant Ga(III) species, the growth of partially crystallized GaOOH thin films with a typical thickness of about 1 μm proceeds. These findings show the correlation between the characteristics of the chemical bath and the resulting structural morphology of GaOOH deposits. They further open great perspectives to grow GaOOH and hence Ga_2O_3-based materials on silicon with a dedicated structural morphology using chemical bath deposition for engineering devices in the fields of gas sensing, solar-blind UV-C photo-detection, and power electronics.

CONFLICTS OF INTEREST

There are no conflicts to declare.

ASSOCIATED CONTENT

Texture coefficients (C_{hkl}) and degree of preferred orientation (σ) of α-GaOOH microrods obtained by CBD for a pH_0 value of 2.26 (Table S1); FESEM-EDS spectra of partially crystallized α-GaOOH thin films grown by CBD (Figure S1).

ACKNOWLEDGMENTS

The authors acknowledge the financial support from the French National Research Agency through the DOSETTE project (ANR-17-CE24-0003). This work has further benefited from some of the characterization equipments of Grenoble INP-CMTC platform. It has partially been supported by the French National Research Agency in the framework of the "Investissement d'Avenir" program (ANR-15-IDEX-02) through the project CDP POWER-ALPS.

REFERENCES

1. Pearton, S. J.; Yang, J.; Cary, P. H.; Ren, F.; Kim, J.; Tadjer, M. J.; Mastro, M. A. A Review of Ga_2O_3 Materials, Processing, and Devices. *Appl. Phys. Rev.* **2018**, *5*, 011301.
2. Galazka, Z. β-Ga_2O_3 for Wide-Bandgap Electronics and Optoelectronics. *Semicond. Sci. Technol.* **2018**, *33*, 113001.
3. Chen, X.; Ren, F.; Gu, S.; Ye, J. Review of Gallium-Oxide-Based Solar-Blind Ultraviolet Photodetectors. *Photon. Res.* **2019**, *7*, 381-415.
4. Green, A. J.; Speck, J.; Xing, G.; Moens, P.; Allerstam, F.; Gumaelius, K.; Neyer, T.; Arias-Purdue, A.; Mehrotra, V.; Kuramata, A.; Sasaki, K.; Watanabe, S.; Koshi, K.; Blevin, J.; Bierwagen, O.;

Krishnamoorthy, S.; Leedy, K.; Arehart, A. R.; Neal, A. T.; Mou, S.; Ringel, S. A.; Kumar, A.; Sharma, A.; Ghosh, K.; Singisetti, U.; Li, W.; Chabak, K.; Liddy, K.; Islam, A.; Rajan, S.; Graham, S.; Choi, S.; Cheng, Z.; Higashiwaki, M. β-Gallium Oxide Power Electronics. *APL Mater.* **2022**, *10*, 029201.
5. Sasaki, K.; Higashiwaki, M.; Kuramata, A.; Masui, T.; Yamakoshi, S. MBE Grown Ga_2O_3 and Its Power Device Applications. *J. Cryst. Growth* **2013**, *378*, 591-595.
6. Zhang, F. B.; Saito, K.; Tanaka, T.; Nishio, M.; Guo, Q. X. Structural and Optical Properties of Ga_2O_3 Films on Sapphire Substrates by Pulsed Laser Deposition. *J. Cryst. Growth* **2014**, *387*, 96-100.
7. Rafique, S.; Han, L.; Tadjer, M. J.; Freitas, J. A.; Mahadik, N. A.; Zhao, H. Homoepitaxial Growth of β-Ga_2O_3 Thin Films by Low Pressure Chemical Vapor Deposition. *Appl. Phys. Lett.* **2016**, *108*, 182105.
8. Alema, F.; Hertog, B.; Osinsky, A.; Mukhopadhyay, P.; Toporkov, M.; Schoenfeld, W. V. Fast Growth Rate of Epitaxial β–Ga_2O_3 by Close Coupled Showerhead MOCVD. *J. Cryst. Growth* **2017**, *475*, 77-82.
9. Comstock, D. J.; Elam, J. W. Atomic Layer Deposition of Ga_2O_3 Films Using Trimethylgallium and Ozone. *Chem. Mater.* **2012**, *24*, 4011-4018.
10. Sato, T.; Nakamura, T. Studies of the Crystallisation of Gallium Hydroxide Precipitated from Hydrochloric Acid Solutions by Various Alkalis. *J. Chem. Technol. Biot.* **1982**, *32*, 469-475.
11. Taş, A. C.; Majewski, P. J.; Aldinger, F. Synthesis of Gallium Oxide Hydroxide Crystals in Aqueous Solutions with or without Urea and Their Calcination Behavior. *J. Am. Ceram. Soc.* **2002**, *85*, 1421-1429.
12. Zhao, Y.; Frost, R. L.; Martens, W. N. Synthesis and Characterization of Gallium Oxide Nanostructures Via a Soft-Chemistry Route. *J. Phys. Chem. C* **2007**, *111*, 16290-16299.
13. Qian, H.-S.; Gunawan, P.; Zhang, Y.-X.; Lin, G.-F.; Zheng, J.-W.; Xu, R. Template-Free Synthesis of Highly Uniform α-GaOOH Spindles and Conversion to α-Ga_2O_3 and β-Ga_2O_3. *Cryst. Growth Des.* **2008**, *8*, 1282-1287.
14. Krehula, S.; Ristić, M.; Kubuki, S.; Iida, Y.; Fabián, M.; Musić, S. The Formation and Microstructural Properties of Uniform α-GaOOH Particles and Their Calcination Products. *J. Alloy Compd* **2015**, *620*, 217-227.
15. Huang, E.; Li, J.; Wu, G.; Dai, W.; Guan, N.; Li, L. A Simple Synthesis of Ga_2O_3 and GaN Nanocrystals. *RSC Adv.* **2017**, *7*, 47898-47903.
16. Chiang, J.-L.; Yadlapalli, B. K.; Chen, M.-I.; Wuu, D.-S. A Review on Gallium Oxide Materials from Solution Processes. *Nanomaterials* **2022**, *12*, 3601.
17. Anastas, P.; Eghbali, N. Green Chemistry: Principles and Practice. *Chem. Soc. Rev.* **2010**, *39*, 301-312.
18. Fujihara, S.; Shibata, Y.; Hosono, E. Chemical Deposition of Rodlike GaOOH and β-Ga_2O_3 Films Using Simple Aqueous Solutions. *J. Electrochem. Soc.* **2005**, *152*, C764.
19. Liang, H.; Meng, F.; Lamb, B. K.; Ding, Q.; Li, L.; Wang, Z.; Jin, S. Solution Growth of Screw Dislocation Driven α-GaOOH Nanorod Arrays and Their Conversion to Porous $ZnGa_2O_4$ Nanotubes. *Chem. Mater.* **2017**, *29*, 7278-7287.
20. Hector, G.; Appert, E.; Sarigiannidou, E.; Matheret, E.; Roussel, H.; Chaix-Pluchery, O.; Consonni, V. Chemical Synthesis of β-Ga_2O_3 Microrods on Silicon and Its Dependence on the Gallium Nitrate Concentration. *Inorg. Chem.* **2020**, *59*, 15696-15706.
21. Berbenni, V.; Milanese, C.; Bruni, G.; Marini, A. Thermal Decomposition of Gallium Nitrate Hydrate $Ga(NO_3)_3 \times xH_2O$. *J. Therm. Anal. Calorim.* **2005**, *82*, 401-407.
22. Zhao, Y.; Yang, J.; Frost, R. L. Raman Spectroscopy of the Transition of α-Gallium Oxyhydroxide to β-Gallium Oxide Nanorods. *J. Raman Spectrosc.* **2008**, *39*, 1327-1331.
23. Welch, M. D.; Kleppe, A. K. Polymorphism of the Hydroxide Perovskite $Ga(OH)_3$ and Possible Proton-Driven Transformational Behaviour. *Phys. Chem. Miner.* **2016**, *43*, 515-526.
24. Benézéth, P.; Diakonov, I. I.; Pokrovski, G. S.; Dandurand, J.-L.; Schott, J.; Khodakovsky, I. L. Gallium Speciation in Aqueous Solution. Experimental Study and Modelling: Part 2. Solubility of α-GaOOH in Acidic Solutions from 150 to 250°C and Hydrolysis Constants of Gallium (III) to 300°C. *Geochim. Cosmochim. Ac.* **1997**, *61*, 1345-1357.
25. Xu, S.; Wang, Z. L. One-Dimensional ZnO Nanostructures: Solution Growth and Functional Properties. *Nano Res.* **2011**, *4*, 1013-1098.

26. Greene, L. E.; Yuhas, B. D.; Law, M.; Zitoun, D.; Yang, P. D. Solution-Grown Zinc Oxide Nanowires. *Inorg. Chem.* **2006**, *45*, 7535-7543.
27. Parize, R.; Garnier, J. D.; Appert, E.; Chaix-Pluchery, O.; Consonni, V. Effects of Polyethylenimine and Its Molecular Weight on the Chemical Bath Deposition of ZnO Nanowires. *ACS Omega* **2018**, *3*, 12457-12464.
28. Liu, B.; Zeng, H. C. Hydrothermal Synthesis of ZnO Nanorods in the Diameter Regime of 50 nm. *J. Am. Chem. Soc.* **2003**, *125*, 4430-4431.
29. Yahiro, J.; Kawano, T.; Imai, H. Nanometric Morphological Variation of Zinc Oxide Crystals Using Organic Molecules with Carboxy and Sulfonic Groups. *J. Colloid Inter. Sci.* **2007**, *310*, 302-311.
30. Shi, F.; Qiao, H. Preparations, Properties and Applications of Gallium Oxide Nanomaterials – a Review. *Nano Select* **2022**, *3*, 348-373.
31. Li, L.; Wei, W.; Behrens, M. Synthesis and Characterization of α-, β-, and Γ-Ga_2O_3 Prepared from Aqueous Solutions by Controlled Precipitation. *Solid State Sci.* **2012**, *14*, 971-981.
32. Kashchiev, D.; van Rosmalen, G. M. Review: Nucleation in Solutions Revisited. *Cryst. Res. Technol.* **2003**, *38*, 555-574.
33. Villafuerte, J.; Sarigiannidou, E.; Donatini, F.; Kioseoglou, J.; Chaix-Pluchery, O.; Pernot, J.; Consonni, V. Modulating the Growth of Chemically Deposited ZnO Nanowires and the Formation of Nitrogen- and Hydrogen-Related Defects Using pH Adjustment. *Nanoscale Adv.* **2022**, *4*, 1793-1807.
34. Lausecker, C.; Salem, B.; Baillin, X.; Consonni, V. Modeling the Elongation of Nanowires Grown by Chemical Bath Deposition Using a Predictive Approach. *J. Phys. Chem. C* **2019**, *123*, 29476-29483.

TOC Graphic

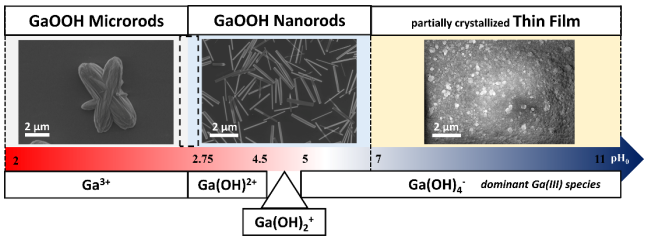

Synopsis

We show that the structural morphology of GaOOH deposits using chemical bath deposition on silicon is tunable from microrods through prismatic nanorods to partially crystallized thin film by adjusting the pH value. The formation process is correlated with the nature of dominant Ga(III) species and the supersaturation level in the chemical bath. These findings open great perspectives to fabricate engineering devices made of GaOOH and Ga_2O_3-based materials using wet chemical route.